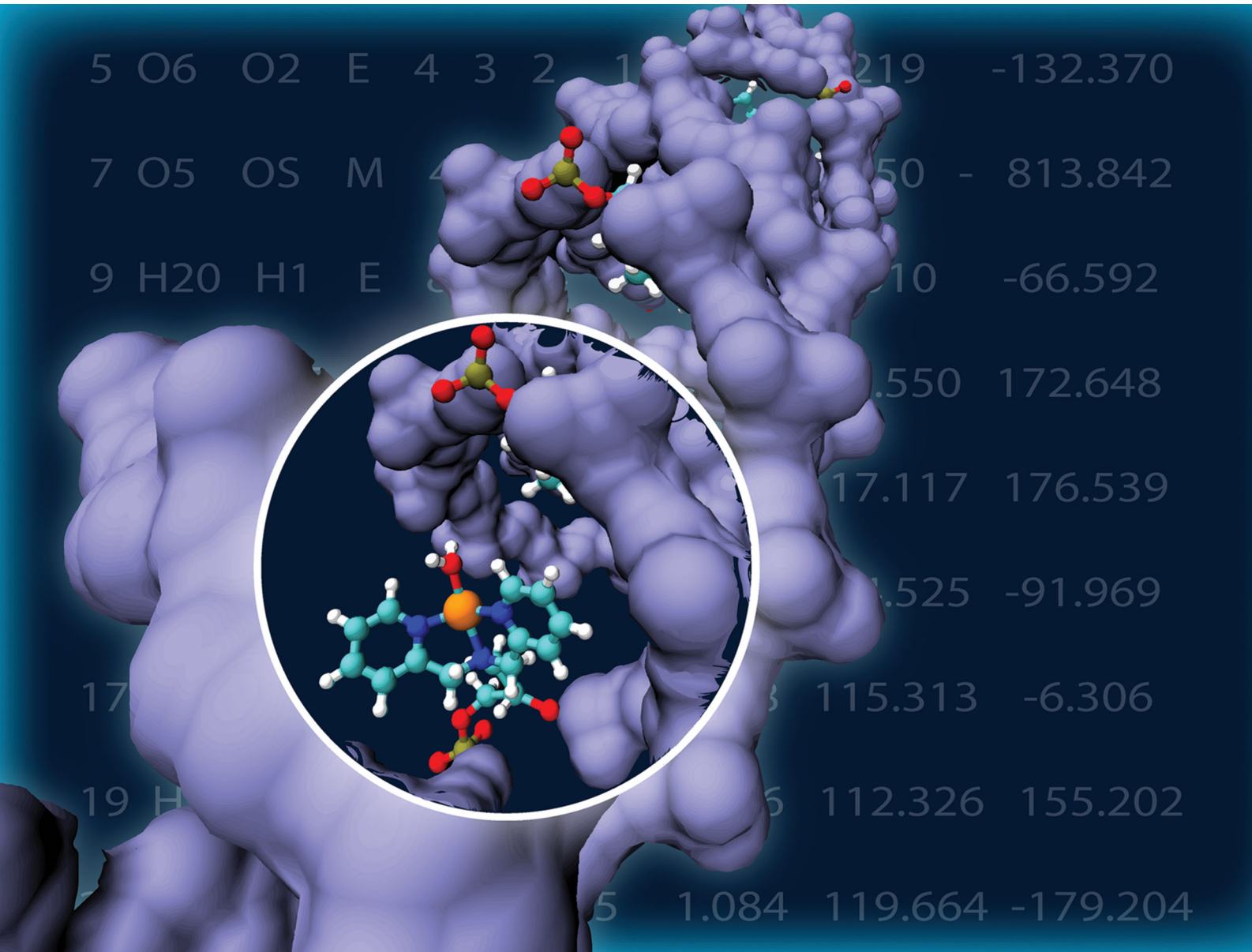


PCCP

Physical Chemistry Chemical Physics

rsc.li/pccp



ISSN 1463-9076

PAPER

Junmei Wang, Sunil Saxena *et al.*

Orientation and dynamics of Cu²⁺ based DNA labels from force field parameterized MD elucidates the relationship between EPR distance constraints and DNA backbone distances



Cite this: *Phys. Chem. Chem. Phys.*,
2020, 22, 26707

Orientation and dynamics of Cu²⁺ based DNA labels from force field parameterized MD elucidates the relationship between EPR distance constraints and DNA backbone distances[†]

Shreya Ghosh,^a Joshua Casto,^{ID a} Xiaowei Bogetti,^a Charu Arora,^a Junmei Wang^{*b} and Sunil Saxena^{ID *a}

Pulsed electron paramagnetic resonance (EPR) based distance measurements using the recently developed Cu²⁺-DPA label present a promising strategy for measuring DNA backbone distance constraints. Herein we develop force field parameters for Cu²⁺-DPA in order to understand the features of this label at an atomic level. We perform molecular dynamics (MD) simulations using the force field parameters of Cu²⁺-DPA on four different DNA duplexes. The distance between the Cu²⁺ centers, extracted from the 2 μs MD trajectories, agrees well with the experimental distance for all the duplexes. Further analyses of the trajectory provide insight into the orientation of the Cu²⁺-DPA inside the duplex that leads to such agreement with experiments. The MD results also illustrate the ability of the Cu²⁺-DPA to report on the DNA backbone distance constraints. Furthermore, measurement of fluctuations of individual residues showed that the flexibility of Cu²⁺-DPA in a DNA depends on the position of the label in the duplex, and a 2 μs MD simulation is not sufficient to fully capture the experimental distribution in some cases. Finally, the MD trajectories were utilized to understand the key aspects of the double electron electron resonance (DEER) results. The lack of orientational selectivity effects of the Cu²⁺-DPA at Q-band frequency is rationalized in terms of fluctuations in the Cu²⁺ coordination environment and rotameric fluctuations of the label linker. Overall, a combination of EPR and MD simulations based on the Cu²⁺-DPA labelling strategy can contribute towards understanding changes in DNA backbone conformations during protein–DNA interactions.

Received 22nd September 2020,
Accepted 21st October 2020

DOI: 10.1039/d0cp05016d

rsc.li/pccp

Introduction

The DNA helix has a wide range of sequence dependent conformational variability and internal dynamics that are essential for its role in biological processes.^{1–5} The DNA helix undergoes breathing, bending and twisting motions, as well as fluctuations in the helical groove that impart flexibility to the helix. Such dynamics are crucial in many important physiological processes. For example, sequence-dependent bending of DNA is an important criterion for protein–DNA recognition and the function of several DNA-binding proteins, such as transcription regulators and restriction enzymes. In recent times, electron paramagnetic resonance (EPR) spectroscopy has increasingly become important for measuring such conformational dynamics in DNA.

In particular, distance measurements using pulsed EPR techniques are an important approach for elucidating macromolecular conformations and flexibility.^{6,7} These EPR techniques exploit the dipolar coupling between unpaired electron spins to provide distances in the nanometer range with angstrom-level resolution.^{7–18} Such distance constraints can be employed to probe conformational changes in large and complex systems, such as membrane proteins, chaperones, protein–protein and protein–nucleic acid complexes, that are otherwise inaccessible to other biophysical techniques.^{19–27}

For such measurements, a site-specific labelling^{28–30} of the biomolecule is needed. A wide variety of labels have been developed for this purpose.^{31,32} For nucleic acids, the spin labels are incorporated by the modification of nucleobase,^{33–41} backbone^{42–45} or terminal capping.^{46,47} Nitroxide based labels are commonly used in DNA. Labels, such as the cytidine analogue or C-spin,^{48–50} are highly rigid and provide information on label orientations.^{51–53} More recently, a sterically shielded nitroxide label, known as the G-spin label,⁵⁴ has been reported that is introduced post synthetically. The G-spin label binds non-covalently to an abasic site and is present close to the helix.

^a Department of Chemistry, University of Pittsburgh, PA 15260, USA.

E-mail: sksaxena@pitt.edu

^b Department of Pharmaceutical Sciences, University of Pittsburgh, PA 15206, USA.

E-mail: junmei.wang@pitt.edu

† Electronic supplementary information (ESI) available. See DOI: 10.1039/d0cp05016d

Additionally, distance measurements at physiological temperatures have been made possible by the triarylmethyl (TAM) radical.^{55,56} Moreover, paramagnetic spin labels such as Mn²⁺, Gd³⁺ and Cu²⁺ have also been used to label nucleic acids.^{57–60}

One such labelling strategy that has shown promise is a Cu²⁺ ion chelated to the ligand 2,2'-dipicolylamine (DPA) phosphoramidite.⁶¹ The DPA moiety is nucleotide independent and can be easily introduced at any desired positions in the duplex during DNA synthesis. In addition, the label is structure independent and thus, does not depend on any specific combinations of bases to bind to, such as a guanine quadruplex. The complementary site to the Cu²⁺-DPA in the opposing strand contains an abasic site (dSpacer). We recently reported distance measurements performed on several duplexes that were labelled at two sites with the Cu²⁺-DPA.⁶² The experimental most probable distances agreed with the predicted distances using the known values of base pair separation for a B-DNA. Moreover, molecular dynamics (MD) simulations performed on an unlabelled DNA also suggested that the most probable distance measured from the experiment agreed with the corresponding C3'-C3' or C4'-C4' backbone distances. These results suggest that the most probable distances obtained using Cu²⁺-DPA labels can be used to report on the DNA backbone conformations in solution.⁶²

However, EPR distance measurements provide sparse constraints and therefore, benefit from complementary techniques, such as atomistic MD simulations. MD simulations including the spin labels combined with EPR distance constraints have provided valuable information on the conformational dynamics of nucleic acids, relative orientation of double-stranded helices and flexibility of DNA for a specific sequence.^{53,54,63–65} Such MD simulations can also provide insight into the global (DNA) and local (spin label) motions. The development of accurate force fields for the spin label is, however, a pre-requisite for such MD simulations.

In this work, we have developed force field parameters for Cu²⁺-DPA and its complementary base, dSpacer. Density functional theory (DFT) calculations were utilized to generate the optimized geometry of Cu²⁺-DPA and the dSpacer. Subsequently, parameters of bond lengths, bond angles, dihedral angles, partial charges, and force constants were developed. We then performed MD simulations with these force fields to better understand the atomic details of the flexibility of DNA as well as the label, Cu²⁺-DPA. The simulations were performed on duplexes with base pair separations of 9 to 12 between the Cu²⁺-DPA labels. We ran the MD simulations for as long as 2 μ s to sample the label dynamics that occur on long timescales. These long simulations provide insight into the shape and width of the experimental distance distributions that were observed in Cu²⁺-DPA labelled DNA,^{62,66} the experimental methodology used to measure distances by EPR, and the spatial distribution of the Cu²⁺-DPA label in the context of the DNA.

Experimental

HYSCORE

Four-pulse hyperfine sublevel correlation (HYSCORE)⁶⁷ experiments were performed at 20 K and at X-band frequencies.

The pulse sequence $\pi/2-\tau-\pi/2-t1-\pi-t2-\pi/2-\tau$ -echo was used. HYSCORE was performed at the field of highest intensity. The initial time delays for τ , $t1$ and $t2$ were set at 128, 200 and 200 ns, respectively. The delay for $t1$ and $t2$ had a step size of 16 ns for a total of 256 points. The pulse lengths used were 16 ns and 32 ns for $\pi/2$ and π pulses, respectively. A four-step phase cycling was used to eliminate the unwanted echos.^{68,69} The raw 2D time-domain signals were analysed and processed using the Hyscorean open-source software package⁷⁰ in MATLAB to produce the 2D frequency-domain contour plot.

DFT optimization

The Cu²⁺ ion is coordinated to three nitrogen atoms of the DPA in the equatorial plane. Therefore, the remaining sites in the Cu²⁺-DPA complex can be occupied by one, two or three water molecules, depending on the geometry. To find out the most possible Cu²⁺-DPA structure, we performed *ab initio* calculations using DFT with the solvent effect being taken into account with the Polarizable Continuum Model implemented in the Gaussian 16 software package.⁷¹ We first conducted geometry optimizations at the wB97xd/6-311++G(2d,p) level for three possible Cu²⁺-DPA complexes with 1, 2 and 3 coordinated water molecules. The complexation energy of introducing a water molecule to a Cu²⁺-DPA complex was then calculated. After the most probable Cu²⁺-DPA complex was identified, we performed vibrational frequency analysis to derive the bond stretching and bond angle bending force constants for the complex at the B3LYP/6-31G* level after geometry optimization. Lastly, HF/6-31G* single point calculations were performed to generate electrostatic potentials (ESP) for the restrained ESP charge fitting. All zero-point energy (ZPE) calculations were performed using the same DFT model as optimization. More information on partial charges, atom types and other force field parameters and residue topologies of the Cu²⁺-DPA is provided in the ESI.†

MD simulations

First, the Nucleic Acid Builder (NAB) module in the AMBER software suite⁷² was used to create the unlabelled B-DNA models, with Cu²⁺-DPA and dSpacer positions replaced by adenine and thymine, respectively. The adenine and thymine residues at the specific sites were then replaced by the DFT-optimized structures of Cu²⁺-DPA and dSpacer in PyMOL.⁷³ The Cu²⁺-DPA and dSpacer incorporated DNA were then subjected to MD simulations. The AMBER parmbsc1 force field⁶³ was used to treat the nucleic acids. For the modified nucleotide residue, we first developed force field parameters for a model compound as shown in Fig. 1, using a strategy detailed previously.⁷⁴ The residue topologies and the key force field parameters of Cu²⁺-DPA and dSpacer are provided in the ESI.† The solvent water was treated using the TIP3P water model.⁷⁵ The DNA duplexes were solvated in a 12 Å truncated octahedral water box. For each DNA duplex, 100 Cl⁻ ions were added to the water box so that the final Cl⁻ concentration is about 0.15 M and the counter Na⁺ ions were then added to neutralize the whole system. The energy minimization and molecular dynamics simulations were performed using the pmemd program

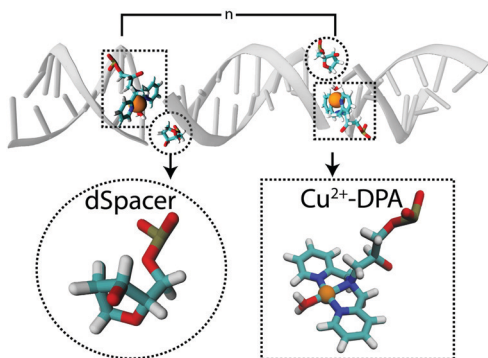


Fig. 1 Cu^{2+} -DPA-DNA duplex with the Cu^{2+} -DPA motif (highlighted by a rectangle) and the dSpacer (highlighted by a circle). The base pair separation between the two Cu^{2+} -DPA motifs is denoted by n .

in the AMBER16 software package.⁷⁶ The solvated systems were first energy-minimized with a harmonic restraint force applied to the DNA residues except for the Cu^{2+} -DPA and dSpacer. The restraint force was gradually reduced from 20, to 10, 5, 1 and finally to 0 kcal mol⁻¹ Å⁻². The systems were then gradually heated from 50, to 100, 150, 200, 250 and finally to 298.15 K. The systems were equilibrated for 2 ns before starting the production MD runs. The time step for the integration of heating, equilibration and the production run was set to 2 fs. Periodic boundary conditions along with particle mesh Ewald (PME)⁷⁷ were applied to account for long-range electrostatic interactions under NPT ($P = 1$ atm) conditions. SHAKE⁷⁸ was used to restrain all bonds involving hydrogen and a nonbonded cutoff of 10 Å was applied. All visualizations for simulations were done using VMD.⁷⁹

Results and discussion

In this work, we systematically examined four Cu^{2+} -DPA-DNA duplexes using MD simulations. Fig. 1 shows a Cu^{2+} -DPA-DNA duplex with two Cu^{2+} -DPA motifs, one on each strand, and a dSpacer, complementary to the Cu^{2+} -DPA. The base pair separations (n) between the Cu^{2+} -DPA motifs were monotonically increased from 9 to 12. The distance distributions on these duplexes have been reported previously.⁶²

DFT optimized structure agrees well with crystal structure

We first identified the most probable structure from three possible Cu^{2+} -DPA complexes with 1, 2 or 3 water molecules, using high-level DFT-optimizations at the wb97xd/6-311++G(2d,p) level. The optimized geometries are shown in Fig. 2. We observed that Cu^{2+} -DPA-WAT₃ is not stable as one Cu-OH₂ distance is 3.988 Å (Fig. 2A), and this water molecule is likely a solvent water. The complexation energy of adding one water to Cu^{2+} -DPA to form Cu^{2+} -DPA-WAT₁ (Fig. 2C) is -19.59 kcal mol⁻¹ and -16.99 kcal mol⁻¹ after ZPE correction. On the other hand, the energy after adding another water molecule in Cu^{2+} -DPA-WAT₂ (Fig. 2B) is only -8.06 kcal mol⁻¹ and -5.86 kcal mol⁻¹ after ZPE correction. Considering that the vaporization energy of water is -9.75 kcal mol⁻¹, Cu^{2+} -DPA-WAT₂ is unlikely to be

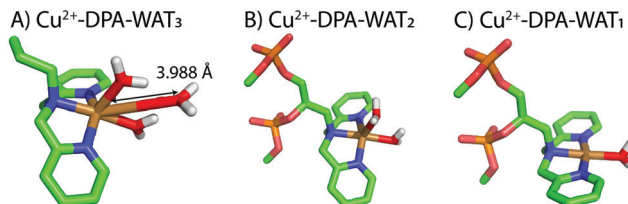


Fig. 2 Cu^{2+} -DPA structures coordinated with (A) three, (B) two and (C) one water molecule.

formed in an aqueous solvent. Thus, the most probable Cu^{2+} -DPA structure contains only one water molecule.

Besides water, the most probable Cu^{2+} -DPA complex, as shown in Fig. 3A, also has the Cu^{2+} coordinated to three nitrogen atoms of the DPA (N1, N2 and N3), similar to what the crystal structure showed.⁸⁰ Previous continuous wave EPR data on Cu^{2+} -DPA-DNA^{61,62} have reported g_{\parallel} and A_{\parallel} values that were also consistent with three nitrogens coordinating to Cu^{2+} at equatorial positions. On comparing the bond lengths and bond angles between the DFT-optimized and crystal structures, we found a reasonable agreement, as shown in Fig. 3B. Furthermore, the optimized geometry did not accommodate any axial water coordination. This absence of axial water coordination indicates a square planar geometry of Cu^{2+} -DPA that is in accordance with the crystal structure.⁸⁰

HYSCORE indicates the presence of the fourth equatorially coordinating atom

In order to experimentally verify the equatorial water coordination to Cu^{2+} -DPA and Cu^{2+} -DPA placed in DNA, we performed HYSCORE experiments. Fig. 4A shows the ¹H HYSCORE spectrum of Cu^{2+} -DPA which displays two proton features. First, the broad ridge spanning a width of 6–9 MHz, highlighted by the rectangles in Fig. 4A, is a characteristic feature of solvent coordination in the equatorial plane.^{81–84} Since three of the equatorial coordination sites of Cu^{2+} are occupied with DPA nitrogen atoms, there is space for only one solvent molecule to bind equatorially. Second, the short intense ridge around the proton Larmor frequency (~ 14 MHz), highlighted by the circle in Fig. 4A, can be a consequence of weakly coupled protons of solvent molecules or axial coordination to water.⁸² Since the crystal structure of Cu^{2+} -DPA shows a square planar geometry,⁸⁰

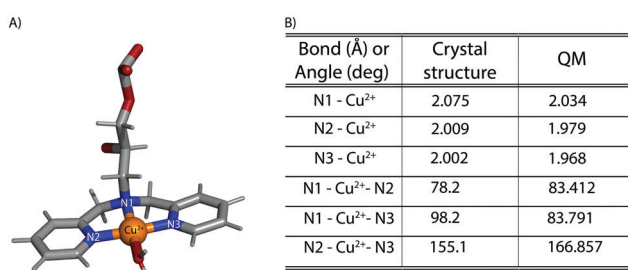


Fig. 3 (A) DFT optimized structure of Cu^{2+} -DPA. (B) Comparison of bond angles and bond lengths with a crystal structure⁸⁰ of Cu^{2+} -DPA shows a reasonable agreement with the DFT-optimized structure.

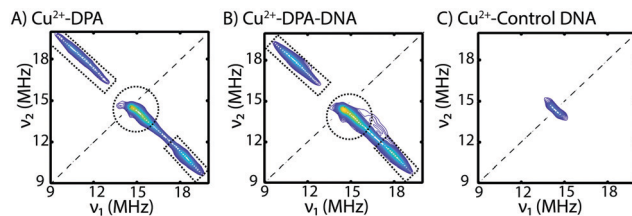


Fig. 4 ^1H HYSCORE spectra of (A) Cu^{2+} -DPA, (B) Cu^{2+} -DPA-DNA and (C) Cu^{2+} -control DNA, analysed to the same contour levels. In Cu^{2+} -DPA and Cu^{2+} -DPA-DNA, the proton signal results from an equatorially coordinated water molecule (rectangle) and a weakly coupled solvent (circle). In control DNA, the proton signal results from only weakly coupled solvent molecules.

the proton feature at ~ 14 MHz is likely due to the weakly coupled protons of solvent molecules.⁸³ We then performed HYSCORE on one of the Cu^{2+} -DPA-DNA duplexes ($n = 11$). The HYSCORE spectrum of the Cu^{2+} -DPA-DNA duplex, shown in Fig. 4B, closely resembles that of the Cu^{2+} -DPA, showing both the features of equatorial water coordination and weakly coupled solvent molecules. Furthermore, a Cu^{2+} -proton distance of 2.5 Å was estimated from the HYSCORE features (details in the ESI†). This distance is in good agreement with the 2.4 Å Cu^{2+} -proton distance in the DFT-optimized structure.

To compare how Cu^{2+} coordination to water differs in the presence and absence of DPA inside the DNA duplex, we performed HYSCORE on a Cu^{2+} -bound control DNA, lacking any DPA phosphoramidite or dSpacer. The sequence of the control DNA is the same as the Cu^{2+} -DPA-DNA duplex, except that the Cu^{2+} -DPA and dSpacer positions were replaced by adenine and thymine, respectively. The proton signature in the HYSCORE spectrum, shown in Fig. 4C, clearly lacks the features of equatorial water coordination as seen in Cu^{2+} -DPA-DNA. Instead,

the spectrum only shows the short intense ridge around ~ 14 MHz. Overall, from the HYSCORE spectra, we inferred that the Cu^{2+} -DPA is coordinated to a solvent molecule in the equatorial plane, as also observed in the DFT-optimized Cu^{2+} -DPA structure.

MD simulations show that the Cu^{2+} - Cu^{2+} distance reasonably agrees with the backbone distance

Next, we performed $2\ \mu\text{s}$ MD simulations on the Cu^{2+} -DPA and dSpacer incorporated into the DNA duplexes, with n varying from 9 to 12. Fig. 5A shows the Cu^{2+} -DPA phosphoramidite with the backbone carbon atom, C' marked in red. The corresponding Cu^{2+} - Cu^{2+} and C' - C' distances in a Cu^{2+} -DPA-DNA duplex are shown using solid black and dashed red lines, respectively. We chose C' as the backbone atom for the Cu^{2+} -DPA phosphoramidite as it is the central point to which the DPA moiety is attached. Moreover, the C' atom best represents the $\text{C}3'$ or $\text{C}4'$ backbone atoms of an unmodified regular nucleotide.⁶²

Fig. 5B–E show the comparison between the Cu^{2+} - Cu^{2+} and C' - C' distance distributions obtained from $2\ \mu\text{s}$ trajectories for each DNA duplex. Fig. 5F shows a plot of the most probable Cu^{2+} - Cu^{2+} and C' - C' distances from the MD. As can be seen, all the distances agree well within ~ 2 Å. The plot, therefore, highlights that an important advantage of the Cu^{2+} -DPA labelling strategy is that the label can reasonably report on the DNA backbone constraints, without any additional modelling.

The agreement between the Cu^{2+} and backbone C' distance distributions is due to a combination of three factors. First, the size of the linker is much smaller than standard DNA labels. From the MD simulations, the average length of the Cu^{2+} atom from the C' backbone atom ranges from 3.5 to 4.5 Å for the different DPA sites. The linker length in Cu^{2+} -DPA is, therefore,

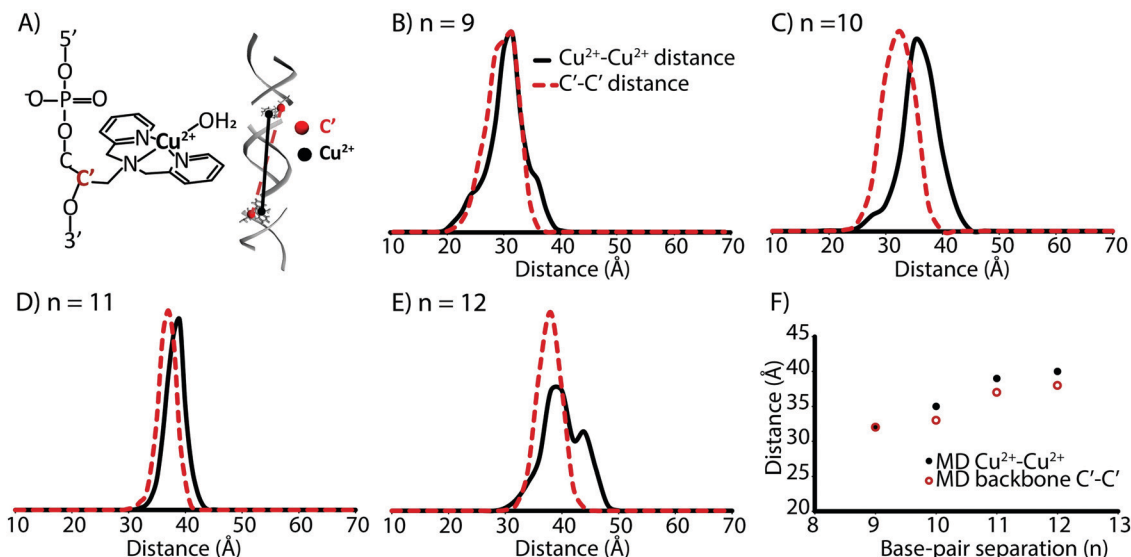


Fig. 5 (A) Cu^{2+} -DPA phosphoramidite with the backbone carbon atom, C' marked in red. The Cu^{2+} - Cu^{2+} distance is denoted by the black solid line and the backbone C' - C' distance is represented by the red dashed line in a Cu^{2+} -DPA-DNA duplex. The Cu^{2+} - Cu^{2+} distance (black solid) is compared with the backbone distance (red dashed) for (B) $n = 9$, (C) $n = 10$, (D) $n = 11$ and (E) $n = 12$ base pair separations. (F) Plot showing the Cu^{2+} - Cu^{2+} and C' - C' most probable distances from MD simulations.

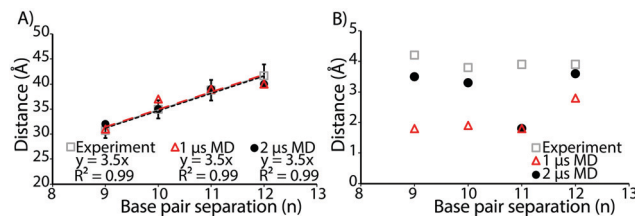


Fig. 6 Plot of (A) most probable Cu^{2+} – Cu^{2+} distances and (B) standard deviation of distance distributions from EPR measurements (grey squares), 1 μs MD (red triangles) and 2 μs MD (black circles) against base pair separation (n). A direct comparison of the experimental and MD distance distributions is provided in the ESI.†

considerably smaller than traditional labels, which can be a nanometer long.^{85,86} Second, the Cu^{2+} is arranged within the helix (*cf.* below). As a result, the offset due to the linker partially cancels. Finally, the Cu^{2+} – Cu^{2+} distance within the DNA helix can be considered as a sum of two components: an axial distance, which increases linearly with the base pair separation and a radial distance (*i.e.* from backbone to the label), which oscillates with base pair separation. As the two modified sites are separated by at least 9 base pairs, the axial vector (~ 31 Å for $n = 9$) is significantly longer than the radial counterpart, *i.e.*, the Cu^{2+} – Cu^{2+} distance is dominated by the axial component. Indeed, previous work has shown that such considerations are valid for $n > 4$.⁶² Consequently, the separation between the Cu^{2+} centers along the DNA axis is roughly the same as the separation between the DNA backbone atoms.

Cu^{2+} -DPA-DNA based MD simulations capture the experimental most probable distance

Next, we compared the distance distributions obtained from MD simulations to the experimental distance distributions. The experimental data and distance distributions for 9 to 12 base pair separations have been reported previously.⁶² The direct comparison of the experimental and MD distance distribution

is provided in the ESI.† Fig. 6A shows the comparison of the most probable Cu^{2+} – Cu^{2+} distances from the first 1 μs (red triangles) and entire 2 μs (black circles) MD simulations and EPR data (grey squares) for the four Cu^{2+} -DPA-DNA duplexes. The distances agree well within 2 Å which is within the error of the experiments.⁶² A linear trend with a y -intercept of 0 was obtained with a slope of 3.5 Å, for all the results from the experiment and MD simulations. These values agree well with each other as well as with the ~ 3.4 Å separation between adjacent bases, as observed in a B-DNA duplex.⁸⁷

Fig. 6B shows the comparison of the standard deviation of the distance distributions obtained from the experimental data (grey squares) and MD simulations (red triangles for 1 μs and black circles for 2 μs). Analysing the initial 1 μs MD trajectories shows a large discrepancy between the experiment and MD for all the duplexes. Extending the simulation time to 2 μs reduces this discrepancy for duplexes $n = 9, 10$ and 12 . However, for duplex $n = 11$, there is no improvement with simulation time. This result may indicate that the labels in duplex $n = 11$ have restricted mobility, and therefore limited sampling of rotamers is observed during the 2 μs simulation. This effect is analysed in further detail below. Overall, while longer simulation time may be required to capture the full distribution width, the most probable distance can be achieved with a short simulation time of 1 μs or less (details in the ESI†).

Orientation of Cu^{2+} -DPA helps reduce the effect of linker offset

To elucidate spin label conformations that yield the most probable distance, we extracted the frames from the MD trajectories for which the Cu^{2+} – Cu^{2+} distance is within ± 1 Å of the MD most probable distance. The analysis is shown in Fig. 7A. Each frame was aligned with respect to the O–C–C'–O backbone atoms, marked in red in Fig. 7B. Fig. 7C and D show the spatial distribution of Cu^{2+} for the DPA sites corresponding to the most probable distance. As can be seen from Fig. 7D, the Cu^{2+} is directed towards the axis of the DNA duplex.

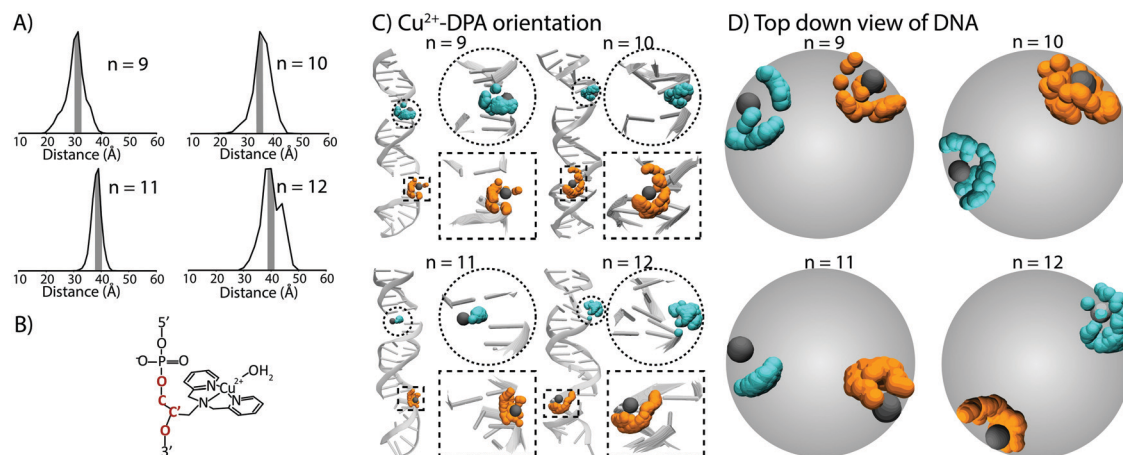


Fig. 7 (A) The frames from MD trajectories considered for obtaining the spatial distribution of Cu^{2+} are within ± 1 Å of the Cu^{2+} – Cu^{2+} most probable distance and shown by the shaded region. (B) The frames are aligned with respect to the Cu^{2+} -DPA backbone atoms marked in red. (C) The distribution of the Cu^{2+} centers for the Cu^{2+} -DPA site 1 (blue, circles) and site 2 (orange, rectangles) for duplexes $n = 9$ – 12 . (D) The top-down view of the DNA where the blue and orange spheres represent the Cu^{2+} at Cu^{2+} -DPA sites 1 and 2, respectively. The grey sphere represents the backbone carbon atom, C'.

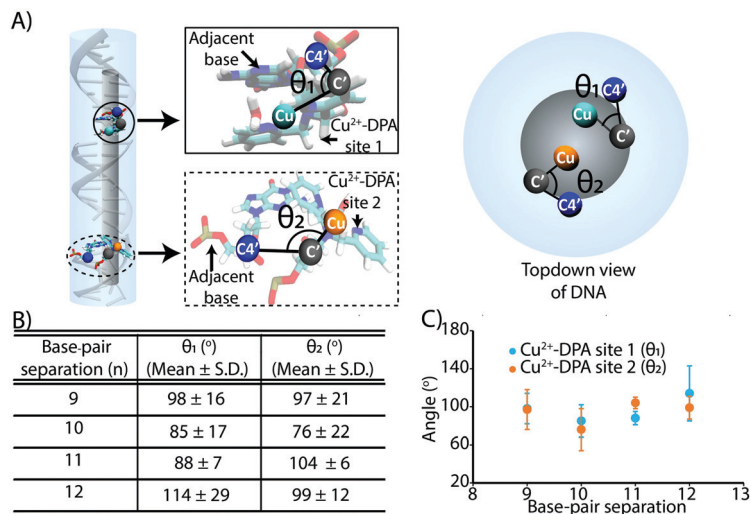


Fig. 8 (A) Angles between the C4' atom of the adjacent base and the Cu²⁺-DPA (blue sphere), the C' backbone atom of Cu²⁺-DPA (grey sphere) and the Cu²⁺ (cyan and orange for Cu²⁺-DPA site 1 and 2, respectively), (B) table showing the values of the angles for the two Cu²⁺-DPA sites, and (C) plot of the angles versus base pair separation for the two Cu²⁺-DPA sites.

This orientation of the Cu²⁺ significantly contributes to the close agreement between the Cu²⁺-Cu²⁺ and backbone distance distributions (*cf.* Fig. 7D).

In addition, we measured the angle between the DNA backbone and the Cu²⁺ for both the sites in the duplex, as shown in Fig. 8A. Fig. 8B shows the value of these angles for the different duplexes. Within the standard deviation, the values agree well with each other. Fig. 8C shows that the average Cu²⁺ to backbone angles for each duplex are all between 80° and 100°. For a natural base, a similar analysis shows an angle of $\sim 73^\circ \pm 6^\circ$ with respect to the backbone atom (details provided in the ESI†). Thus, the Cu²⁺-DPA orientation to the DNA backbone is roughly similar to that of a natural base within the standard deviation and within the caveats of structural differences between the label and the natural base. These results suggest that the most probable spin label conformation has the Cu²⁺-ions present almost perpendicular to the DNA backbone. The perpendicular orientation of the Cu²⁺-DPA leads to the effects of linker length partially cancelling out when the Cu²⁺-Cu²⁺ distance is compared to the backbone distance.

MD simulations show that Cu²⁺-DPA has varied mobility that depends on position

In order to examine the motion of the Cu²⁺-DPA, we first measured the root mean square fluctuation (RMSF) values of each base for all the DNA duplexes. The RMSF was calculated with reference to the average structure of each duplex and the results are shown in Fig. 9. As expected, the bases at the 5' and 3' ends showed high RMSF and therefore, high flexibility. Interestingly, the flexibility of the Cu²⁺-DPA and the dSpacer is also elevated compared to other bases and is comparable to the nitroxide derivative of guanine.⁵⁴ These results are expected because Cu²⁺-DPA and the dSpacer lack intrastrand hydrogen bonding between them unlike regular base pairing. Importantly, the difference in the RMSF value between DPA and the

adjacent base is small for $n = 11$. Furthermore, the RMSF values in Fig. 9 are consistent with the fluctuations in θ_1 and θ_2 (*cf.* Fig. 8B).

We analysed the spin label rotameric preferences from the MD trajectories to examine the mobility of the DPA in different sites. The Cu²⁺-DPA moiety is connected to the backbone by two rotatable bonds that are defined here by χ_1 and χ_2 . These angles are shown in Fig. 10A and 11A, respectively. The χ_1 dihedral angles for both the Cu²⁺-DPA sites in each duplex are shown in Fig. 10B-E. In duplexes $n = 9, 10$ and 12 , at least one of the Cu²⁺-DPA sites sample both $\pm 60^\circ$ and $\pm 180^\circ$, while in $n = 11$ neither of the labels sample the full range. Fig. 11B-E show the χ_2 dihedral angles for both the Cu²⁺-DPA sites in each duplex. Overall, a large range of χ_2 values ($\pm 60^\circ, \pm 120^\circ$ and $\pm 180^\circ$) are sampled between the different Cu²⁺-DPA sites of the different

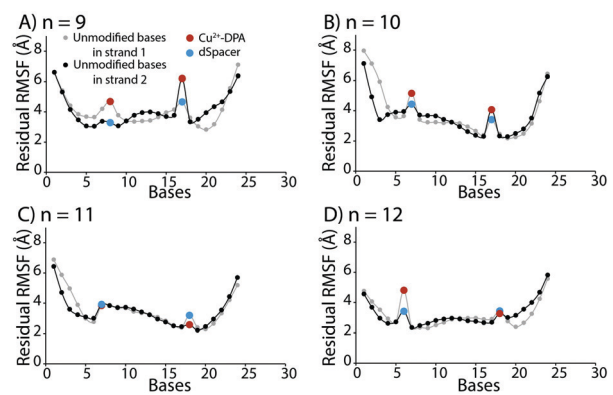


Fig. 9 The root mean square fluctuations (RMSFs) of all the bases in the Cu²⁺-DPA-DNA duplexes with (A) $n = 9$, (B) $n = 10$, (C) $n = 11$ and (D) $n = 12$. The grey and black denote the two strands in the DNA and the red and blue denote Cu²⁺-DPA and dSpacer, respectively. As can be seen, the RMSF is high for the terminal bases, as expected. The RMSFs for Cu²⁺-DPA and the abasic dSpacer positions are generally high, indicating more flexibility than the natural bases.

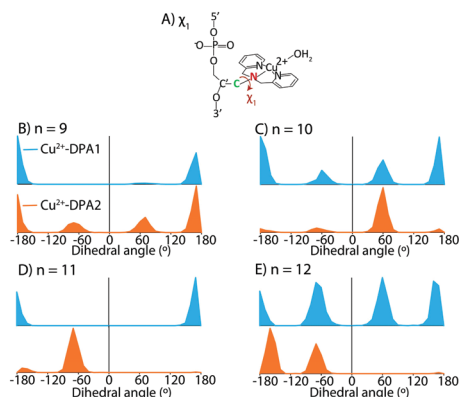


Fig. 10 (A) Dihedral angle denoted as χ_1 . The probability distribution of the dihedral angles for the two Cu^{2+} -DPA labels in duplexes with (B) $n = 9$, (C) $n = 10$, (D) $n = 11$ and (E) $n = 12$. Both the Cu^{2+} -DPA sites in the duplex $n = 11$ sample the least range of χ_1 dihedrals.

duplexes. These observations suggest that the sampling of χ_1 and χ_2 dihedral angles contributes towards the flexibility of the label in a duplex, and that $n = 11$ does not fully sample all rotameric states during the course of MD simulation.

Moreover, as evident from Fig. 10 and 11, even within the same duplex, two Cu^{2+} -DPA sites can have varied mobility. Such differences in the mobility depending on the location of the Cu^{2+} -DPA site are not unreasonable given that local steric interactions with the neighbouring bases have a strong influence on the degree of motions of the label.

Finally, these results suggest that a $2\ \mu\text{s}$ simulation may be insufficient, in such cases, to fully capture the experimental distribution due to the slow motion of the label.^{33,88–90} In addition, there may be contributions from other factors that lead to the discrepancy between the distribution widths in MD simulations vs. the experiment. The experimental data were collected at 20 K which is likely to capture the conformations that exist in the glass state, while the simulation was performed at 298 K. Second, glycerol was used in the experiment to form a

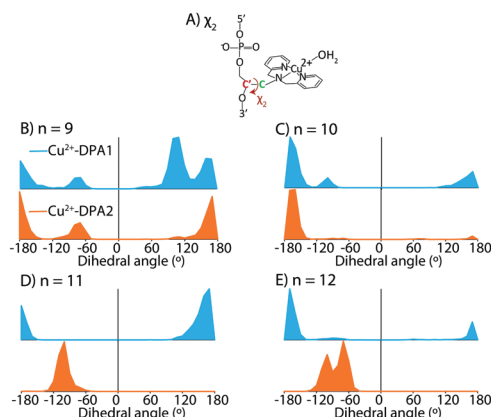


Fig. 11 (A) Dihedral angle denoted as χ_2 . (B) Energy landscape for different orientations of Cu^{2+} -DPA based on the dihedral angle, χ_2 . The probability distribution of the dihedral angles for the two Cu^{2+} -DPA labels in duplexes with (C) $n = 9$, (D) $n = 10$, (E) $n = 11$ and (F) $n = 12$.

glass and as a cryoprotectant. It is possible that the presence of glycerol modified the solvation and dynamics of the DNA.^{91,92}

MD simulations provide insight into the use of DEER for distance measurements

The MD results are also helpful to understand key principles of the double electron electron resonance (DEER) measurements on Cu^{2+} -DPA labelled species. The pulses used in DEER excite only a small fraction of the total EPR spectrum. Such selective excitation can lead to the selection of only a small portion of all possible molecular orientations, resulting in the dependence of the measured signal on the magnetic field. This is often referred to as orientational selectivity.^{59,93–101} Previous DEER results have shown the absence of orientational effects for Cu^{2+} -DPA at both X-band and Q-band frequencies in the non-complexed state.^{61,62} This is intriguing because Cu^{2+} -based measurements on proteins using the dHis motif^{74,93,102–104} can be orientationally selective at the Q-band but not at the X-band.

We examined the MD data to gain insight into these observations. Fig. 12 shows the fluctuations of the bond lengths for bonds involving Cu^{2+} . These bond lengths were extracted from the $2\ \mu\text{s}$ MD trajectory on the $n = 11$ duplex since previous Q-band data on this sample did not exhibit orientational selectivity.⁶² The bond length between Cu^{2+} and N1 ranges from 1.9 to 2.3 Å, with an average bond length of 2.1 ± 0.1 Å (average \pm s.d.). On the other hand, the bond length of Cu^{2+} to N2 was 1.9 ± 0.1 Å. These mean values agree well with the crystal structure⁸⁰ (cf. Fig. 3). Fig. 13 shows the dihedral angles between Cu^{2+} and atoms in its immediate coordination environment. The dihedral angles, labelled as N1, N2 and N3, show values of $-75^\circ \pm 23^\circ$, $-20^\circ \pm 7^\circ$ and $19^\circ \pm 6^\circ$ (average \pm s.d.), respectively, and are similar for the two Cu^{2+} -DPA sites. The ensemble measured by DEER is therefore expected to contain proteins trapped in these different coordination environments.

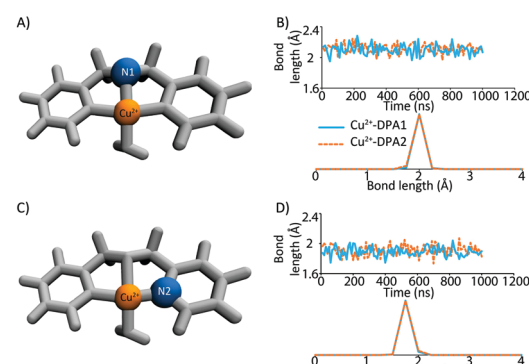


Fig. 12 Fluctuations in bond length between Cu^{2+} and the two coordinating nitrogen atoms – (A) bond between Cu^{2+} and the backbone N1 atom, (B) fluctuations in Cu^{2+} -N1 bond length in the two DPA sites, sampled over $2\ \mu\text{s}$ of MD for the duplex $n = 11$ (top chart) and the probability distribution (bottom chart), and (C) and (D) the same analysis repeated for bond length between Cu^{2+} and the pyridine N2 atom. A change of $\sim 25\%$ in the bond length is observed for Cu^{2+} -N1 and $\sim 30\%$ for Cu^{2+} -N2.

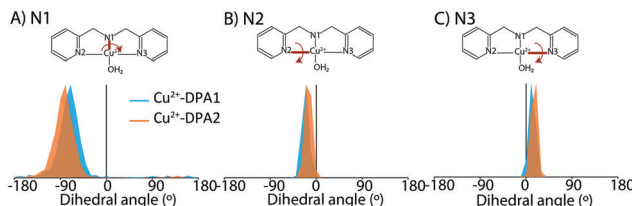


Fig. 13 Dihedral angles measured between Cu^{2+} and its coordinating atoms for 2 μs of MD run on the Cu^{2+} -DPA-DNA duplex with $n = 11$. The dihedral angle is denoted by the red arrow (top chart). The bottom chart shows the probability distribution of the dihedrals between the two Cu^{2+} -DPA sites, Cu^{2+} -DPA1 (blue) and Cu^{2+} -DPA2 (orange).

Such variations in the coordination environment of Cu^{2+} have a significant influence on the g -tensor of the label. Accordingly, we calculated the g -tensor values and orientations for 100 snapshots from our MD using ORCA.^{105,106} For these calculations, we sampled every 10 ns of the first 1 μs trajectory of duplex $n = 11$. The distribution in g_{\parallel} orientations shows dramatic variations with as much as a 25° change, as shown in cyan in Fig. 14. Due to its 180° symmetry,^{93,97} the g_{\parallel} orientations show both 'up' and 'down' orientations with respect to the plane of the Cu^{2+} -DPA moiety. This is not unexpected and has been observed before.^{93,97} In addition to this distribution of g_{\parallel} in the two Cu^{2+} centers, there is also additional contribution due to the fluctuations of the dihedral angles χ_1 and χ_2 (cf. Fig. 10 and 11).

Together these two effects have significant implications on the relative orientations of the g -tensors of the two Cu^{2+} spins in the DNA duplex. The relative angles of the two g -tensors are defined by three angles that are shown in Fig. 15A. χ is the angle between the g_{\parallel} axis and the interspin vector, r . γ is the angle between the g_{\parallel} axis of spin A and its projection on spin B. η is the angle between the g_{\perp} axis of spin A and its projection on spin B.

The three angles, namely χ , γ , and η , were calculated *via* the MDTraj software¹⁰⁷ for 100 snapshots of the Cu^{2+} -DPA-DNA duplex with $n = 11$. From our analysis, we obtained an average of $103^\circ \pm 69^\circ$ (average \pm s.d.), $87^\circ \pm 36^\circ$ and $93^\circ \pm 44^\circ$ for χ , η and γ , respectively. Similar analysis of angles for the dHis- Cu^{2+} protein label has shown a standard deviation of $\sim 10\text{--}12^\circ$ for each set of angles.^{74,93} Thus, the Cu^{2+} -DPA labels have an

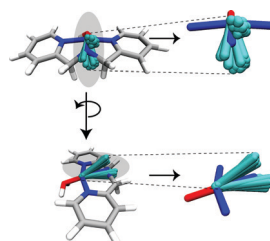


Fig. 14 The distribution of g_{\parallel} directions (cyan) in the Cu^{2+} -DPA system, sampled every 10 ns of the 1 μs MD run. The blue and red bonds show the Cu^{2+} coordination with nitrogen and oxygen, respectively. The cyan represents the g_{\parallel} . The g -tensor calculations were performed with ORCA.^{105,106}

orientational distribution that is significantly larger compared to the dHis- Cu^{2+} label used for proteins. The key distinguishing feature appears to be the smaller contribution from side-chain fluctuations in the dHis motif.^{74,93}

We utilized the values of χ , γ , and η angles and performed simulations to obtain individual time-domain DEER signals at various magnetic fields using the methodology reported previously.¹⁰⁸ The parameters used for the simulations include the g and hyperfine tensor values for Cu^{2+} -DPA ($g_{\parallel} = 2.247$, $g_{\perp} = 2.054$, $A_{\parallel} = 170$ G and $A_{\perp} = 17$ G⁶²). We also used the experimental most probable distance of 3.78 nm and a standard deviation of 0.38 nm for the distance distribution for duplex $n = 11$. Fig. 15B shows the eight different magnetic fields where we have previously reported DEER for $n = 11$ ⁶² and where the simulations are carried out in this work. As can be seen from Fig. 15C, the simulated DEER time traces have the same period at all fields. Furthermore, Fig. 15D shows that there is no difference in the dipolar frequency at the g_{\perp} (11 820 G) and g_{\parallel} (11 220 G) regions, indicating the lack of any orientational selectivity effects at Q-band frequency.

Many orientations are excited even at a single magnetic field

In order to visualize how the effects of orientational selectivity are mitigated, we chose one Cu^{2+} centre as the reference and aligned its g_{\parallel} axis to overlay 100 structures of Cu^{2+} -DPA-DNA, evenly sampled from the 1 μs MD simulations. Fig. 16 shows the locations of the second Cu^{2+} (orange) and the reference Cu^{2+} center is shown as a black sphere. As is evident from the figure, even at a single magnetic field corresponding to g_{\parallel} , there are a large number of molecular orientations that can exist. In general, the finite bandwidth of the pump pulse in DEER leads to an excitation of an even wider range of molecular

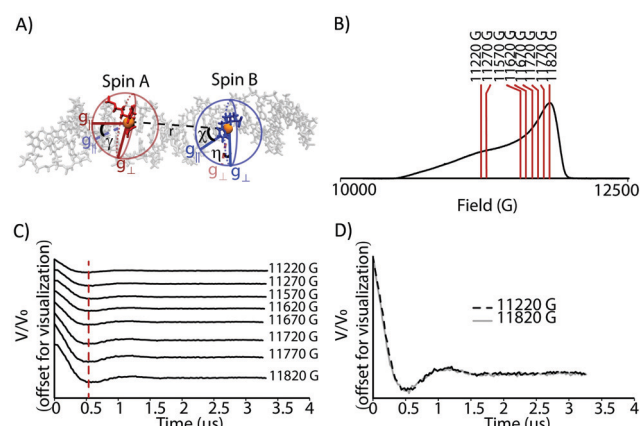


Fig. 15 (A) The relative orientations between the two spins, A and B, are indicated by three angles, χ , γ and η . (B) The echo-detected field swept spectrum of the Cu^{2+} -DPA-DNA duplex with $n = 11$ at Q-band frequency. The red lines show the fields at which DEER was simulated. (C) The simulated DEER time traces at each field at the Q-band frequency. The y-axis is offset for visualization. The red dashed line represents the first period of the modulations for all fields. (D) Background subtracted time domain data at g_{\parallel} (11 220 G, dashed) and g_{\perp} (11 820 G, solid) regions. The figure shows the lack of orientational selectivity effects at Q-band frequency for Cu^{2+} -DPA.

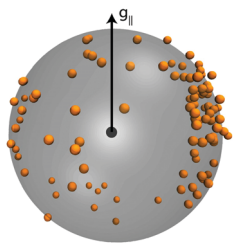


Fig. 16 MD frames of the Cu^{2+} -DPA-DNA duplex ($n = 11$) sampled every 10 ns for the first 1 μs . The black sphere in the center is the reference Cu^{2+} . All frames are aligned to the g_{\parallel} axis of the reference Cu^{2+} . The second Cu^{2+} position is represented as orange spheres. The g_{\parallel} direction, marked in the figure, is calculated from ORCA.^{105,106}

orientations at a particular magnetic field. Such occurrence is a combined consequence of fluctuations in the dihedral angles, χ_1 and χ_2 and in the coordination environment of Cu^{2+} leading to a large distribution in the g -tensor orientations.

Conclusions

In conclusion, we have, for the first time, provided tools for modelling Cu^{2+} -DPA by developing force field parameters. The DFT-optimized structure of the label was in reasonable agreement with the crystal structure. Additionally, the most energy favourable DFT-structure had one equatorial water coordination and was consistent with the HYSCORE results on the Cu^{2+} -DPA-DNA duplex. We have shown that the distance between the Cu^{2+} centers from the MD simulations can directly report on the DNA backbone distances. In addition, the most probable Cu^{2+} - Cu^{2+} distance obtained from the experiment and the MD agree within ~ 2 \AA . Further analyses showed that the Cu^{2+} -DPA moiety is positioned inside the DNA helix and oriented roughly perpendicular to the DNA backbone. The motions of the label are slow such that simulation longer than 2 μs may be needed, in such cases, to adequately capture the experimental distance distribution. Finally, the MD results illustrated that the fluctuations of the Cu^{2+} coordination environment, together with the linker flexibility, lead to a wide distribution of the relative orientation of the two Cu^{2+} g -tensors. This distribution is large enough to dilute any orientational effects, even at Q-band frequency. Overall, the development of force field parameters for the Cu^{2+} labels will enable the use of MD simulations to better interpret EPR distance constraints in understanding the role of DNA in protein-DNA interactions.

Conflicts of interest

There are no conflicts to declare.

Acknowledgements

This research was supported by the National Science Foundation [NSF-BSF MCB-2006154 to S. S., NSF 1955260 to J. W.] and

the National Institutes of Health [NIH: P30 DA035778 to J. W.]. S. G. would like to thank the University of Pittsburgh for the Andrew Mellon Predoctoral Fellowship. We would also like to thank Dr Lillian Chong and Anthony Bogetti for the useful discussions on M. D. simulations. All simulations were carried out at the University of Pittsburgh's Center for Research Computing.

References

- 1 S. C. Parker, L. Hansen, H. O. Abaan, T. D. Tullius and E. H. Margulies, Local DNA topography correlates with functional noncoding regions of the human genome, *Science*, 2009, **324**, 389–392.
- 2 R. Rohs, S. M. West, A. Sosinsky, P. Liu, R. S. Mann and B. Honig, The role of DNA shape in protein-DNA recognition, *Nature*, 2009, **461**, 1248–1253.
- 3 S. Harteis and S. Schneider, Making the bend: DNA tertiary structure and protein-DNA interactions, *Int. J. Mol. Sci.*, 2014, **15**, 12335–12363.
- 4 G. W. Reginsson, S. A. Shelke, C. Rouillon, M. F. White, S. T. Sigurdsson and O. Schiemann, Protein-induced changes in DNA structure and dynamics observed with noncovalent site-directed spin labeling and PELDOR, *Nucleic Acids Res.*, 2013, **41**, e11.
- 5 O. A. Krumkacheva, G. Y. Shevelev, A. A. Lomzov, N. S. Dyrkheeva, A. A. Kuzhelev, V. V. Koval, V. M. Tormyshev, Y. F. Polienko, M. V. Fedin, D. V. Pyshnyi, O. I. Lavrik and E. G. Bagryanskaya, DNA complexes with human apurinic/apyrimidinic endonuclease 1: structural insights revealed by pulsed dipolar EPR with orthogonal spin labeling, *Nucleic Acids Res.*, 2019, **47**, 7767–7780.
- 6 P. P. Borbat and J. H. Freed, in *Biological Magnetic Resonance*, ed. C. Timmel and J. Harmer, Kluwer Academic/Plenum Publishers, New York, 2000, pp. 1–82.
- 7 G. Jeschke, DEER distance measurements on proteins, *Annu. Rev. Phys. Chem.*, 2012, **63**, 419–446.
- 8 A. D. Milov, A. G. Maryasov and Y. D. Tsvetkov, Pulsed electron double resonance (PELDOR) and its applications in free-radicals research, *Appl. Magn. Reson.*, 1998, **15**, 107–143.
- 9 S. Ruthstein, M. Ji, B. K. Shin and S. Saxena, A simple double quantum coherence ESR sequence that minimizes nuclear modulations in Cu^{2+} -ion based distance measurements, *J. Magn. Reson.*, 2015, **257**, 45.
- 10 M. Ji, S. Ruthstein and S. Saxena, Paramagnetic metal ions in pulsed ESR distance distribution measurements, *Acc. Chem. Res.*, 2014, **47**, 688–695.
- 11 M. Pannier, S. Veit, A. Godt, G. Jeschke and H. W. Spiess, Dead-Time Free Measurement of Dipole-Dipole Interactions between Electron Spins, *J. Magn. Reson.*, 2000, **142**, 331–340.
- 12 S. Saxena and J. H. Freed, Double quantum two-dimensional Fourier transform electron spin resonance: distance measurements, *Chem. Phys. Lett.*, 1996, **251**, 102–110.

13 L. V. V. Kulik, S. A. A. Dzuba, I. A. A. Grigoryev and Y. D. Tsvetkov, Electron dipole-dipole interaction in ESEEM of nitroxide biradicals, *Chem. Phys. Lett.*, 2001, **343**, 315–324.

14 S. Milikisyants, F. Scarpelli, M. G. Finiguerra, M. Ubbink and M. Huber, A pulsed EPR method to determine distances between paramagnetic centers with strong spectral anisotropy and radicals: the dead-time free RIDME sequence, *J. Magn. Reson.*, 2009, **201**, 48–56.

15 G. Jeschke, M. Pannier, A. Godt and H. W. Spiess, Dipolar spectroscopy and spin alignment in electron paramagnetic resonance, *Chem. Phys. Lett.*, 2000, **331**, 243–252.

16 T. Schmidt, M. A. Wälti, J. L. Baber, E. J. Hustedt and G. M. Clore, Long Distance Measurements up to 160 Å in the GroEL Tetradecamer Using Q-Band DEER EPR Spectroscopy, *Angew. Chem., Int. Ed.*, 2016, **55**, 15905–15909.

17 J. S. Becker and S. Saxena, Double quantum coherence electron spin resonance on coupled Cu(II)–Cu(II) electron spins, *Chem. Phys. Lett.*, 2005, **414**, 248–252.

18 S. Ruthstein, M. Ji, P. Mehta, L. Jen-Jacobson and S. Saxena, Sensitive Cu²⁺–Cu²⁺ Distance Measurements in a Protein–DNA Complex by Double-Quantum Coherence ESR, *J. Phys. Chem. B*, 2013, **117**, 6227–6230.

19 K. M. Stone, J. E. Townsend, J. Sarver, P. J. Sapienza, S. Saxena and L. Jen-Jacobson, Electron spin resonance shows common structural features for different classes of EcoRI-DNA complexes, *Angew. Chem., Int. Ed.*, 2008, **47**, 10192–10194.

20 M. Grote, Y. Polyhach, G. Jeschke, H. Steinhoff, E. Schneider and E. Bordignon, Transmembrane signaling in the maltose ABC transporter MalFGK2-E, *J. Biol. Chem.*, 2009, **284**, 17521–17526.

21 G. Hagelueken, W. J. Ingledew, H. Huang, B. Petrovic-Stojanovska, C. Whitfield, H. Elmaki, O. Schiemann and J. H. Naismith, PELDOR Spectroscopy Distance Fingerprinting of the Octameric Outer-Membrane Protein Wza from *Escherichia coli*, *Angew. Chem., Int. Ed.*, 2009, **48**, 2904–2906.

22 M. Drescher, M. Huber and V. Subramaniam, Hunting the Chameleon: Structural Conformations of the Intrinsically Disordered Protein Alpha-Synuclein, *ChemBioChem*, 2012, **13**, 761–768.

23 B. Joseph, A. Sikora, E. Bordignon, G. Jeschke, D. S. Cafiso and T. F. Prisner, Distance Measurement on an Endogenous Membrane Transporter in *E. coli* Cells and Native Membranes Using EPR Spectroscopy, *Angew. Chem., Int. Ed.*, 2015, **54**, 6196–6199.

24 M. C. Puljung, H. A. DeBerg, W. N. Zagotta and S. Stoll, Double electron-electron resonance reveals cAMP-induced conformational change in HCN channels, *Proc. Natl. Acad. Sci. U. S. A.*, 2014, **111**, 9816–9821.

25 I. D. Sahu, G. Dixit, W. Reynolds, B. Harding, C. Jaycox, F. D. M. Faleel, R. M. McCarrick, C. R. Sanders and G. A. Lorigan, Studying Conformation of the Voltage-Sensor Domain (VSD) of the Human KCNQ1 Potassium Ion Channel in Proteoliposomes using EPR Spectroscopy, *Biophys. J.*, 2019, **116**, 26a.

26 T. Schmidt, C. D. Schwieters and G. M. Clore, Spatial domain organization in the HIV-1 reverse transcriptase p66 homodimer precursor probed by double electron-electron resonance EPR, *Proc. Natl. Acad. Sci. U. S. A.*, 2019, **116**, 17809–17816.

27 A. Giannoulis, A. Feintuch, Y. Barak, H. Mazal, S. Albeck, T. Unger, F. Yang, X. C. Su and D. Goldfarb, Two closed ATP- And ADP-dependent conformations in yeast Hsp90 chaperone detected by Mn(II) EPR spectroscopic techniques, *Proc. Natl. Acad. Sci. U. S. A.*, 2020, **117**, 395–404.

28 W. L. Hubbell, H. S. Mchaourab, C. Altenbach and M. A. Lietzow, Watching proteins move using site-directed spin labeling, *Structure*, 1996, **4**, 779–783.

29 G. Jeschke and Y. Polyhach, Distance measurements on spin-labelled biomacromolecules by pulsed electron paramagnetic resonance, *Phys. Chem. Chem. Phys.*, 2007, **9**, 1895–1910.

30 W. L. Hubbell, C. J. Lopez, C. Altenbach and Z. Yang, Technological advances in site-directed spin labeling of proteins, *Curr. Opin. Struct. Biol.*, 2013, **23**, 725–733.

31 S. A. Shelke and S. T. Sigurdsson, Site-directed spin labeling of nucleic acids, *Eur. J. Org. Chem.*, 2012, 2291–2301.

32 S. A. Shelke and S. T. Sigurdsson, *Modified Nucleic Acids*, Springer, 2016, vol. 31, pp. 159–187.

33 O. Schiemann, N. Piton, Y. Mu, G. Stock, J. W. Engels and T. F. Prisner, A PELDOR-based nanometer distance ruler for oligonucleotides, *J. Am. Chem. Soc.*, 2004, **126**, 5722–5729.

34 G. Scollo, F. Wachowius, M. Bennati and C. Hobartner, Probing secondary structures of spin-labeled RNA by pulsed EPR spectroscopy, *Angew. Chem., Int. Ed.*, 2010, **49**, 6443–6447.

35 E. S. Babaylova, A. V. Ivanov, A. A. Malygin, M. A. Vorobjeva, A. G. Venyaminova, Y. F. Polienko, I. A. Kirilyuk, O. A. Krumkacheva, M. V. Fedin, G. G. Karpova and E. G. Bagryanskaya, A versatile approach for site-directed spin labeling and structural EPR studies of RNAs, *Org. Biomol. Chem.*, 2014, **12**, 3129–3136.

36 S. Saha, A. P. Jagtap and S. T. Sigurdsson, Site-directed spin labeling of 2'-amino groups in RNA with isoindoline nitroxides that are resistant to reduction, *Chem. Commun.*, 2015, **51**, 13142–13145.

37 N. Erlenbach, B. Endeward, P. Schöps, D. B. Gophane, S. T. Sigurdsson and T. F. Prisner, Flexibilities of isoindoline-derived spin labels for nucleic acids by orientation selective PELDOR, *Phys. Chem. Chem. Phys.*, 2016, **18**, 16196–16201.

38 K. Halbmair, J. Seikowski, I. Tkach, C. Hobartner, D. Sezer and M. Bennati, High-resolution measurement of long-range distances in RNA: pulse EPR spectroscopy with TEMPO-labeled nucleotides, *Chem. Sci.*, 2016, **7**, 3172–3180.

39 O. Frolov, B. Endeward, O. Schiemann, T. F. Prisner and J. W. Engels, Nitroxide Spin labeled RNA for long range distance measurements by EPR-PELDOR, *Nucleic Acids Symp. Ser.*, 2008, **52**, 153–154.

40 M. Kerzhner, D. Abdullin, J. Wiecek, H. Matsuoka, G. Hagelueken, O. Schiemann and M. Famulok, Post-synthetic spin-labeling of RNA through click chemistry for PELDOR measurements, *Chem. – Eur. J.*, 2016, **22**, 12113–12121.

41 Q. Cai, A. K. Kusnetzow, W. L. Hubbell, I. S. Haworth, G. P. C. Gacho, N. Van Eps, K. Hideg, E. J. Chambers and P. Z. Qin, Site-directed spin labeling measurements of nanometer distances in nucleic acids using a sequence-independent nitroxide probe, *Nucleic Acids Res.*, 2006, **34**, 4722–4730.

42 P. H. Nguyen, A. Popova, K. Hideg and P. Z. Qin, A nucleotide-independent cyclic nitroxide label for monitoring segmental motions in nucleic acids, *BMC Biophys.*, 2016, **8**, 6–14.

43 A. M. Popova, T. Kálai, K. Hideg and P. Z. Qin, Site-specific DNA structural and dynamic features revealed by nucleotide-independent nitroxide probes, *Biochemistry*, 2009, **48**, 8540–8550.

44 P. Z. Qin, I. S. Haworth, Q. Cai, A. K. Kusnetzow, G. P. G. Grant, E. A. Price, G. Z. Sowa, A. Popova, B. Herreros and H. He, Measuring nanometer distances in nucleic acids using a sequence-independent nitroxide probe, *Nat. Protoc.*, 2007, **2**, 2354–2365.

45 M. M. Haugland, A. H. El-Sagheer, R. J. Porter, J. Pena, T. Brown, E. A. Anderson and J. E. Lovett, 2'-Alkynyl nucleotides: a sequence- and spin label-flexible strategy for EPR spectroscopy in DNA, *J. Am. Chem. Soc.*, 2016, **138**, 9069–9072.

46 G. Y. Shevelev, O. A. Krumkacheva, A. A. Lomzov, A. A. Kuzhelev, D. V. Trukhin, O. Y. Rogozhnikova, V. M. Tormyshev, D. V. Pyshnyi, M. V. Fedin and E. G. Bagryanskaya, Triarylmethyl labels: toward improving the accuracy of EPR nanoscale distance measurements in DNAs, *J. Phys. Chem. B*, 2015, **119**, 13641–13648.

47 M. V. Fedin, G. Y. Shevelev, D. V. Pyshnyi, V. M. Tormyshev, G. Jeschke, M. Yulikov and E. G. Bagryanskaya, Interaction of triarylmethyl radicals with DNA termini revealed by orientation-selective W-band double electron–electron resonance spectroscopy, *Phys. Chem. Chem. Phys.*, 2016, **18**, 29549–29554.

48 N. Barhate, P. Cekan, A. P. Massey and S. T. Sigurdsson, A nucleoside that contains a rigid nitroxide spin label: a fluorophore in disguise, *Angew. Chem., Int. Ed.*, 2007, **46**, 2655–2658.

49 P. Cekan and S. T. Sigurdsson, Conformation and dynamics of nucleotides in bulges and symmetric internal loops in duplex DNA studied by EPR and fluorescence spectroscopies, *Biochem. Biophys. Res. Commun.*, 2012, **420**, 656–661.

50 P. Cekan, A. L. Smith, N. Barhate, B. H. Robinson and S. T. Sigurdsson, Rigid spin-labeled nucleoside C: a non-perturbing EPR probe of nucleic acid conformation, *Nucleic Acids Res.*, 2008, **36**, 5946–5954.

51 T. E. Edwards, P. Cekan, G. W. Reginsson, S. A. Shelke, A. R. Ferré-D'Amaré, O. Schiemann and S. T. Sigurdsson, Crystal structure of a DNA containing the planar, phenoxazine-derived bi-functional spectroscopic probe C, *Nucleic Acids Res.*, 2011, **39**, 4419–4426.

52 A. Marko, V. Denysenkov, D. Margraf, P. Cekan, O. Schiemann, S. T. Sigurdsson and T. F. Prisner, Conformational flexibility of DNA, *J. Am. Chem. Soc.*, 2011, **133**, 13375–13379.

53 L. S. Stelzl, N. Erlenbach, M. Heinz, T. F. Prisner and G. Hummer, Resolving the conformational dynamics of DNA with ångstrom resolution by PELDOR and molecular dynamics, *J. Am. Chem. Soc.*, 2017, **139**, 11674–11677.

54 M. Heinz, N. Erlenbach, L. S. Stelzl, G. Thierolf, N. R. Kamble, S. T. Sigurdsson, T. F. Prisner and G. Hummer, High-resolution EPR distance measurements on RNA and DNA with the non-covalent G spin label, *Nucleic Acids Res.*, 2020, **48**, 924–933.

55 G. Y. Shevelev, O. A. Krumkacheva, A. A. Lomzov, A. A. Kuzhelev, O. Y. Rogozhnikova, D. V. Trukhin, T. I. Troitskaya, V. M. Tormyshev, M. V. Fedin, D. V. Pyshnyi and E. G. Bagryanskaya, Physiological-Temperature Distance Measurement in Nucleic Acid using Triarylmethyl-Based Spin Labels and Pulsed Dipolar EPR Spectroscopy, *J. Am. Chem. Soc.*, 2014, **136**, 9874–9877.

56 A. A. Kuzhelev, O. A. Krumkacheva, G. Y. Shevelev, M. Yulikov, M. V. Fedin and E. G. Bagryanskaya, Room-temperature distance measurements using RIDME and the orthogonal spin labels trityl/nitroxide, *Phys. Chem. Chem. Phys.*, 2018, **20**, 10224–10230.

57 M. P. Donohue and V. A. Szalai, Distance measurements between paramagnetic ligands bound to parallel stranded guanine quadruplexes, *Phys. Chem. Chem. Phys.*, 2016, **18**, 15447–15455.

58 F. Wojciechowski, A. Gross, I. T. Holder, L. Knorr, M. Drescher, J. S. Hartig, A. Groß, I. T. Holder, L. Knorr, M. Drescher and J. S. Hartig, Pulsed EPR spectroscopy distance measurements of DNA internally labelled with Gd³⁺-DOTA, *Chem. Commun.*, 2015, **51**, 13850–13853.

59 D. M. Engelhard, A. Meyer, A. Berndhäuser, O. Schiemann and G. H. Clever, Di-copper(II) DNA G-quadruplexes as EPR distance rulers, *Chem. Commun.*, 2018, **54**, 7455–7458.

60 Y. Song, T. J. Meade, A. V. Astashkin, E. L. Klein, J. H. Enemark and A. Raitsimring, Pulsed dipolar spectroscopy distance measurements in biomacromolecules labeled with Gd(III) markers, *J. Magn. Reson.*, 2011, **210**, 59–68.

61 M. J. Lawless, J. L. Sarver and S. Saxena, Nucleotide independent Cu(II) based distance measurements in DNA by pulsed EPR, *Angew. Chem., Int. Ed.*, 2017, **56**, 2115–2117.

62 S. Ghosh, M. J. Lawless, H. J. Brubaker, K. Singewald, M. R. Kurpiewski, L. Jen-Jacobson and S. Saxena, Cu²⁺-based distance measurements by pulsed EPR provide distance constraints for DNA backbone conformations in solution, *Nucleic Acids Res.*, 2020, **48**, e49.

63 I. Ivani, P. D. Dans, A. Noy, A. Pérez, I. Faustino, A. Hospital, J. Walther, P. Andrio, R. Goñi, A. Balaceanu, G. Portella, F. Battistini, J. L. Gelpí, C. González,

M. Vendruscolo, C. A. Laughton, S. A. Harris, D. A. Case and M. Orozco, Parmbsc1: a refined force field for DNA simulations, *Nat. Methods*, 2016, **13**, 55–58.

64 C. Prior, L. Danilane and V. S. Oganesyan, All-atom molecular dynamics simulations of spin labelled double and single-strand DNA for EPR studies, *Phys. Chem. Chem. Phys.*, 2018, **20**, 13461–13472.

65 A. Gamble Jarvi, A. Sargun, X. Bogetti, J. Wang, C. Achim and S. Saxena, Development of Cu(II)-based distance methods and force field parameters for the determination of PNA conformations and dynamics by EPR and MD simulations, *J. Phys. Chem. B*, 2020, **124**, 7544–7556.

66 M. J. Lawless, J. Sarver and S. Saxena, Nucleotide-independent copper(II)-based distance measurements in DNA by pulsed ESR spectroscopy, *Angew. Chem., Int. Ed.*, 2017, **56**, 2115–2117.

67 S. Van Doorslaer, *eMagRes*, John Wiley & Sons, Ltd, Chichester, UK, 2017, vol. 6, pp. 51–70.

68 J. M. Fauth, A. Schweiger, L. Braunschweiler, J. Forrer and R. R. Ernst, Elimination of Unwanted Echoes and Reduction of Dead Time in Three-Pulse Electron Spin-Echo Spectroscopy, *J. Magn. Reson.*, 1986, **66**, 74–85.

69 C. Gemperle, G. Aebl, A. Schweiger and R. R. Ernst, Phase Cycling in Pulse EPR, *J. Magn. Reson.*, 1990, **88**, 241–256.

70 L. Fábregas Ibáñez, J. Soetbeer, D. Klose, M. Tinzl, D. Hilvert and G. Jeschke, Non-uniform HYSCORE: Measurement, processing and analysis with Hyscorean, *J. Magn. Reson.*, 2019, **307**, 106576.

71 M. J. Frisch, G. W. Trucks, H. B. Sclegel, G. E. Scuseria, M. A. Robb, J. R. Cheeseman, G. Scalmani, V. Barone, G. A. Petersson, H. Nakatsuji, X. Li, M. Caricato, A. V. Marenich, J. Bloino, B. G. Janesko, R. Gomperts, B. Mennucci, H. P. Hratchian, J. V. Ortiz, A. F. Izmaylov, J. L. Sonnenberg, D. Williams-Young, F. Ding, F. Lipparini, F. Egidi, J. Goings, B. Peng, A. Petrone, T. Henderson, D. Ranasinghe, V. G. Zakrzewski, J. Gao, N. Rega, G. Zheng, W. Liang, M. Hada, M. Ehara, K. Toyota, R. Fukuda, J. Hasegawa, M. Ishida, T. Nakajima, Y. Honda, O. Kitao, H. Nakai, T. Vreven, K. Throssell, J. A. Montgomery Jr., J. E. Peralta, F. Ogliaro, M. J. M. J. Bearpark, J. J. Heyd, E. N. Brothers, K. N. Kudin, V. N. Staroverov, T. A. Keith, R. Kobayashi, J. Normand, K. Raghavachari, A. P. Rendell, J. C. Burant, S. S. Iyengar, J. Tomasi, M. Cossi, J. M. Millam, M. Klene, C. Adamo, R. Cammi, J. W. Ochterski, R. L. Martin, K. Morokuma, O. Farkas, J. B. Foresman and D. J. Fox, *Gaussian 16, Revision C.01*, Gaussian Inc, Wallingford, CT, 2016.

72 D. A. Case, T. E. Cheatham III, T. Darden, H. Gohlke, R. Luo, K. M. Merz Jr., A. Onufriev, C. Simmerling, B. Wang and R. J. Woods, The Amber biomolecular simulation programs, *J. Comput. Chem.*, 2005, **26**, 1668–1688.

73 W. L. Delano, *PyMOL: An Open-Source Molecular Graphics Tool*, 2002.

74 X. Bogetti, S. Ghosh, A. Gamble Jarvi, J. Wang and S. Saxena, Molecular Dynamics Simulations Based on Newly Developed Force Field Parameters for Cu²⁺ Spin Labels Provide Insights into Double-Histidine-Based Double Electron-Electron Resonance, *J. Phys. Chem. B*, 2020, **124**, 2788–2797.

75 W. L. Jorgensen, J. Chandrasekhar, J. D. Madura, R. W. Impey and M. L. Klein, Comparison of simple potential functions for simulating liquid water, *J. Chem. Phys.*, 1983, **79**, 926–935.

76 D. Case, R. Betz, W. Botello-Smith, D. Cerutti and T. Darden, *Amber 16*, Univ. California, San Fr, 2016.

77 T. Darden, D. York and L. Pedersen, Particle mesh Ewald: an *N*-log(*N*) method for Ewald sums in large systems, *J. Chem. Phys.*, 1993, **98**, 10089–10092.

78 J. P. Ryckaert, G. Ciccotti and H. J. Berendsen, Numerical integration of the cartesian equations of motion of a system with constraints: molecular dynamics of *n*-alkanes, *J. Comput. Phys.*, 1977, **23**, 327–341.

79 W. Humphrey, A. Dalke and K. Schulten, VMD: visual molecular dynamics, *J. Mol. Graphics*, 1996, **14**, 33–38.

80 K.-Y. Choi, H. Ryu, N.-D. Sung and M. Suh, Synthesis, properties, and X-ray structure of [Cu(dpa)Cl₂] (dpa = di-(2-picoly)amine), *J. Chem. Crystallogr.*, 2003, **33**, 947–950.

81 P. M. Schosseler, B. Wehrli and A. Schweiger, Complexation of Copper(II) with Carbonate Ligands in Aqueous Solution: A CW and Pulse EPR Study, *Inorg. Chem.*, 1997, **36**, 4490–4499.

82 M. G. Santangelo, A. Medina-Molner, A. Schweiger, G. Mitrikas and B. Spingler, Structural analysis of Cu(II) ligation to the 5'-GMP nucleotide by pulse EPR spectroscopy, *J. Biol. Inorg. Chem.*, 2007, **12**, 767–775.

83 C. S. Burns, E. Aronoff-Spencer, C. M. Dunham, P. Lario, N. I. Avdievich, W. E. Antholine, M. M. Olmstead, A. Vrielink, G. J. Gerfen, J. Peisach, W. G. Scott and G. L. Millhauser, Molecular features of the copper binding sites in the octarepeat domain of the prion protein, *Biochemistry*, 2002, **41**, 3991–4001.

84 A. Pöppl and L. Kevan, A practical strategy for determination of proton hyperfine interaction parameters in paramagnetic transition metal ion complexes by two-dimensional HYSCORE electron spin resonance spectroscopy in disordered systems, *J. Phys. Chem.*, 1996, **100**, 3387–3394.

85 D. B. Gophane, B. Endeward, T. F. Prisner and S. T. Sigurdsson, Conformationally Restricted Isoindoline-Derived Spin Labels in Duplex DNA: Distances and Rotational Flexibility by Pulsed Electron-Electron Double Resonance Spectroscopy, *Chem. – Eur. J.*, 2014, **20**, 15913–15919.

86 D. B. Gophane and S. T. Sigurdsson, Hydrogen-bonding controlled rigidity of an isoindoline-derived nitroxide spin label for nucleic acids, *Chem. Commun.*, 2013, **49**, 999–1001.

87 W. K. Olson, A. A. Gorin, X. J. Lu, L. M. Hock and V. B. Zhurkin, DNA sequence-dependent deformability deduced from protein-DNA crystal complexes, *Proc. Natl. Acad. Sci. U. S. A.*, 1998, **95**, 11163–11168.

88 R. Galindo-Murillo, D. R. Roe and T. E. Cheatham, Convergence and reproducibility in molecular dynamics

simulations of the DNA duplex d(GCACGAACGAACGAACGC), *Biochim. Biophys. Acta*, 2015, **1850**, 1041–1058.

89 P. H. von Hippel, N. P. Johnson and A. H. Marcus, 50 years of DNA ‘Breathing’: Reflections on old and new approaches [For special issue of biopolymers on 50 years of nucleic acids research], *Biopolymers*, 2013, **99**, 923–954.

90 M. D. Frank-Kamenetskii and S. Prakash, Fluctuations in the DNA double helix: a critical review, *Phys. Life Rev.*, 2014, **11**, 153–170.

91 E. R. Georgieva, A. S. Roy, V. M. Grigoryants, P. P. Borbat, K. A. Earle, C. P. Scholes, J. H. Freed, M. Grigoryants, P. P. Borbat, K. A. Earle, C. P. Scholes and J. H. Freed, Effect of freezing conditions on distances and their distributions derived from Double Electron Electron Resonance (DEER): a study of doubly-spin-labeled T4 lysozyme, *J. Magn. Reson.*, 2012, **216**, 69–77.

92 R. Sinibaldi, M. G. Ortore, F. Spinozzi, F. Carsughi, H. Frielinghaus, S. Cinelli, G. Onori and P. Mariani, Preferential hydration of lysozyme in water/glycerol mixtures: a small-angle neutron scattering study, *J. Chem. Phys.*, 2007, **126**, 235101.

93 A. Gamble Jarvi, K. Ranguelova, S. Ghosh, R. T. Weber and S. Saxena, On the Use of Q-Band Double Electron–Electron Resonance To Resolve the Relative Orientations of Two Double Histidine-Bound Cu²⁺ Ions in a Protein, *J. Phys. Chem. B*, 2018, **122**, 10669–10677.

94 O. Schiemann, P. Cekan, D. Margraf, T. F. Prisner and S. T. Sigurdsson, Relative Orientation of Rigid Nitroxides by PELDOR: Beyond Distance Measurements in Nucleic Acids, *Angew. Chem., Int. Ed.*, 2009, **48**, 3292–3295.

95 Z. Yang, D. Kise and S. Saxena, An Approach towards the Measurement of Nanometer Range Distances Based on Cu²⁺ Ions and ESR, *J. Phys. Chem. B*, 2010, **114**, 6165–6174.

96 A. Marko, D. Margraf, P. Cekan, S. T. Sigurdsson, O. Schiemann and T. F. Prisner, Analytical method to determine the orientation of rigid spin labels in DNA, *Phys. Rev. E: Stat., Nonlinear, Soft Matter Phys.*, 2010, **81**, 021911.

97 A. M. Bowen, M. W. Jones, J. E. Lovett, T. G. Gaule, M. J. McPherson, J. R. Dilworth, C. R. Timmel and J. R. Harmer, Exploiting orientation-selective DEER: Determining molecular structure in systems containing Cu(II) centres, *Phys. Chem. Chem. Phys.*, 2016, **18**, 5981–5994.

98 V. P. Denysenkov, T. F. Prisner, J. Stubbe and M. Bennati, High-field pulsed electron-electron double resonance spectroscopy to determine the orientation of the tyrosyl radicals in ribonucleotide reductase, *Proc. Natl. Acad. Sci. U. S. A.*, 2006, **103**, 13386–13390.

99 B. E. Bode, J. Plackmeyer, T. F. Prisner and O. Schiemann, PELDOR Measurements on a Nitroxide-Labeled Cu(II) Porphyrin: Orientation Selection, Spin-Density Distribution, and Conformational Flexibility, *J. Phys. Chem. A*, 2008, **112**, 5064–5073.

100 C. Abé, D. Klose, F. Dietrich, W. H. Ziegler, Y. Polyhach, G. Jeschke and H. J. Steinhoff, Orientation selective DEER measurements on vinculin tail at X-band frequencies reveal spin label orientations, *J. Magn. Reson.*, 2012, **216**, 53–61.

101 J. E. Lovett, A. M. Bowen, C. R. Timmel, M. W. Jones, J. R. Dilworth, D. Caprotti, S. G. Bell, L. L. Wong and J. Harmer, Structural information from orientationally selective DEER spectroscopy, *Phys. Chem. Chem. Phys.*, 2009, **11**, 6840.

102 T. F. Cunningham, M. R. Puterman, A. Desai, W. S. Horne and S. Saxena, The Double-Histidine Cu²⁺-Binding Motif: A Highly Rigid, Site-Specific Spin Probe for Electron Spin Resonance Distance Measurements, *Angew. Chem., Int. Ed.*, 2015, **54**, 6330–6334.

103 M. J. Lawless, S. Ghosh, T. F. Cunningham, A. Shimshi and S. Saxena, On the use of the Cu²⁺-iminodiacetic acid complex for double histidine based distance measurements by pulsed ESR, *Phys. Chem. Chem. Phys.*, 2017, **19**, 20959–20967.

104 S. Ghosh, M. J. Lawless, G. S. Rule and S. Saxena, The Cu²⁺-nitrilotriacetic acid complex improves loading of α -helical double histidine site for precise distance measurements by pulsed ESR, *J. Magn. Reson.*, 2018, **286**, 163–171.

105 F. Neese, The ORCA program system, *Wiley Interdiscip. Rev.: Comput. Mol. Sci.*, 2012, **2**, 73–78.

106 F. Neese, Software update: the ORCA program system, version 4.0, *Wiley Interdiscip. Rev.: Comput. Mol. Sci.*, 2018, **8**, e1327.

107 R. T. McGibbon, K. A. Beauchamp, M. P. Harrigan, C. Klein, J. M. Swails, C. X. Hernández, C. R. Schwantes, L. P. Wang, T. J. Lane and V. S. Pande, MDTraj: A Modern Open Library for the Analysis of Molecular Dynamics Trajectories, *Biophys. J.*, 2015, **109**, 1528–1532.

108 Z. Yang, D. Kise and S. Saxena, An approach towards the measurement of nanometer range distance based on Cu²⁺ ions and ESR, *J. Phys. Chem. B*, 2010, **114**, 6165–6174.